Probing Surface Band Bending of Surface-Engineered Metal Oxide Nanowires

Cheng-Ying Chen,[†,‡] Jose Ramon Duran Retamal,[†] I-Wen Wu,[†] Der-Hsien Lien,[‡] Ming-Wei Chen,[†] Yong Ding,[‡] Yu-Lun Chueh,[§] Chih-I Wu,[†] and Jr-Hau He[†,*]

[†]Institute of Photonics and Optoelectronics and Department of Electrical Engineering, National Taiwan University, Taipei 10617, Taiwan, ROC, [‡]School of Material Science and Engineering, Georgia Institute of Technology, Atlanta, Georgia 30332, United States, and [§]Department of Materials Science and Engineering, National Tsing Hua University, Hsinchu 30013, Taiwan, ROC

ABSTRACT We *in situ* probed the surface band bending (SBB) by ultraviolet photoelectron spectroscopy (UPS) in conjunction with field-effect transistor measurements on the incompletely depleted ZnO nanowires (NWs). The diameter range of the NWs is *ca.* 150−350 nm. Several surface treatments (*i.e.*, heat treatments and Au nanoparticle (NP) decoration) were conducted to assess the impact of the oxygen adsorbates on the SBB. A 100 °C heat treatment leads to the decrease of the SBB to 0.74 ± 0.15 eV with 29.9 ± 3.0 nm width, which is attributed to the removal of most adsorbed oxygen molecules from the ZnO NW surfaces. The SBB of the oxygen-adsorbed ZnO NWs is measured to be 1.53 ± 0.15 eV with 43.2 ± 2.0 nm width. The attachment of Au NPs to the NW surface causes unusually high SBB (2.34 ± 0.15 eV with the wide width of 53.3 ± 1.6 nm) by creating open-circuit nano-Schottky junctions and catalytically enhancing the formation of the charge O_2 adsorbates. These surface-related phenomena should be generic to all metal oxide nanostructures. Our study is greatly beneficial for the NW-based device design of sensor and optoelectronic applications *via* surface engineering.

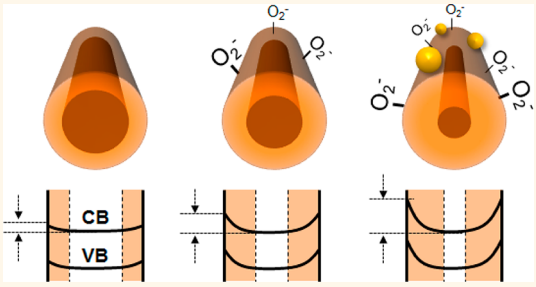

KEYWORDS: ZnO · metal oxide · nanowire · surface band bending · Schottky junction · oxygen vacancy

Nanowires (NWs) have attracted extensive attention due to their importance in fundamental research and potential applications in nanoscale electronics and optoelectronics.[1−8] With large surface-to-volume ratios and Debye lengths comparable to their diameters, the electronic and the optoelectronic properties of NWs are strongly affected by the surface effect[1] *via* chemisorption/photodesorption[2,4,9−11] and native surface defects/states.[12] Accordingly, one-dimensional (1-D) nanostructures exhibit a superior sensitivity to light/chemical molecules, as compared to their thin film counterpart.[13−17] Moreover, the surface modification of NWs can enhance the sensitivity to light/chemical molecules due to an enhanced surface effect and can be achieved by surface functionalization, polymer coating, metal doping, and nanoparticle (NP) decoration.[1,4,6]

It is speculated that surface band bending (SBB) is invoked into the surface effect, but only circumstantial evidence for the presence of SBB has been provided *via* transport, gas sensing, photon sensing, and field-effect transistor (FET) measurements.[1,3,5,6] Moreover, the usefulness of electrical measurements, such as current−voltage (*IV*) and capacitance−voltage (*CV*) analyses, is limited as the electrode contacts are needed and might irreversibly cause damage to NWs, leading to mis-estimation during analysis.[12,18−22] Accordingly, correctly evaluating the SBB of NWs is essential to understand the 1-D transport physics and further explore the device performance limits. Furthermore, the ultraviolet photoemission spectroscopy (UPS) enables the non-invasive inspection of the most superficial properties for the NW (1−3 nm),[23] so a change of surface potential can be sensed easily through measuring a parallel shift of all binding energies by the UPS.

In this study, we employed the UPS analyses in conjunction with the FET measurements to probe the SBB of ZnO NWs.

* Address correspondence to jhhe@ntu.edu.tw.

Received for review December 28, 2011 and accepted October 24, 2012.

Published online October 24, 2012
10.1021/nn205097e

© 2012 American Chemical Society

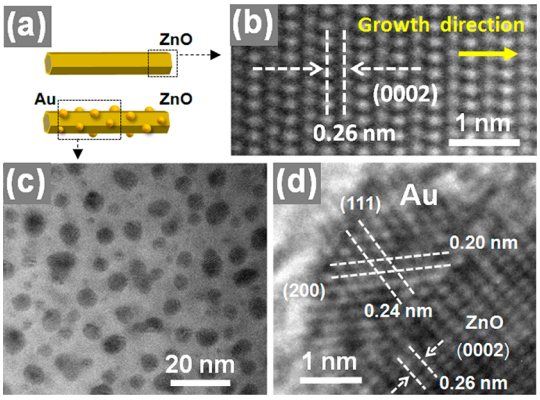

Figure 1. (a) Schematic of a *c*-axis-oriented ZnO NW with Au NP decoration, (b) HRTEM image of a ZnO NW, (c) TEM image of an Au NP-decorated ZnO NW, and (d) HRTEM image at the interface of Au NPs and a ZnO NW.

Systematic surface treatments were conducted to assess the impact of the oxygen adsorbates on the SBB; we "engineer" the valence band maximum (E_V) of the ZnO NW surface through heat treatments and Au NPs. The SBB of the oxygen-adsorbed ZnO NWs is measured to be 1.53 ± 0.15 eV with 43.2 ± 2.0 nm width. A 100 °C heat treatment for removing most of the adsorbed oxygen molecules from the NW surfaces leads to a decrease of the SBB to 0.74 ± 0.15 eV with 29.9 ± 3.0 nm width. The introduction of Au NPs to ZnO NW surfaces increases the quantity of adsorbed oxygen molecules by creating open-circuit nano-Schottky junctions and catalytically enhancing the reaction of the O_2 into adsorbates, giving rise to an increase of the SBB to 2.34 ± 0.15 eV with 53.3 ± 1.6 nm width. These surface-related phenomena should be inherited by all metal oxide nanostructures. A quantitative understanding of the SBB facilitates broad applications in NW-based electronics and optoelectronics where surface engineering is needed to optimize the device efficiencies and functionalities.

RESULTS AND DISCUSSION

It is known that the grain boundaries in polycrystalline oxide materials form the depletion layers, which significantly influence measured electronic structures. Therefore, it is essential to characterize the microstructures of NWs to make sure that NWs are single-crystalline, and thus the surface plays a consistent and dominant role in electronic properties of the ZnO NW material system in this study. Transmission electron microscopy (TEM) is used in the microstructure analysis, as shown in Figure 1. The high-resolution TEM (HRTEM) shows that the NWs are single-crystalline (Figure 1b). The interplanar distance of 0.26 nm corresponds to the ZnO (0002) planes, showing that the NWs grow along the *c* axis.[24] After the Au deposition, Au NPs with the sizes of a few nanometers (dark spherical regions) were formed (Figure 1c), with a coverage ratio of ~40% over the ZnO NW surface. Figure 1d shows a cross-sectional HRTEM image of the junction between Au and ZnO. The interplanar distances are 0.20 and 0.24 nm, corresponding to Au(200) and Au(111) planes, respectively. By examining the interface of Au and ZnO in Figure 1d, no intermediate phase between Au and ZnO has been observed, indicating that no chemical reaction occurs after the Au deposition.

The undoped ZnO is an n-type semiconductor due to its intrinsic defects, such as oxygen deficiencies.[12,25] The defects in the surface layer readily act as the adsorption sites. The gas molecules, such as O_2, tend to be chemisorbed on the ZnO surface by capturing free electrons [$O_2(g) + e^- \rightarrow O_2^-(ad)$]. As a result, the adsorbates acting as acceptors reduce the free carrier density and thus deplete the surface electron states, leading to the formation of the space charge region and the band bending near the NW surface. It has been speculated that the SBB of NWs is related to NW diameter,[26] doping level,[26] surface roughness,[27] and molecule adsorption[9,27]/metal decoration[28−30] on NW surfaces. As considering the diameter and the doping only, a qualitative description of the energy difference, ϕ, produced by SBB obeys the following equations:[26]

$$\phi \propto eN_d d^2/\varepsilon_r\varepsilon_0 \quad \text{for } d \le d_{crit} \quad \text{(for a completely depleted NW)} \qquad (1)$$

and

$$\phi \propto eN_d d^2{}_{crit}/\varepsilon_r\varepsilon_0 \quad \text{for } d > d_{crit} \quad \text{(for an incompletely depleted NW)} \qquad (2)$$

where N_d is the donor concentration (cm^{-3}), d is the NW diameter, d_{crit} is the critical diameter of the NWs, ε_r is the dielectric constant of the NWs, and ε_0 is the permittivity of free space. For the NWs with $d > d_{crit}$, the value of ϕ is no longer a function of diameter, and thus their SBB is identical. Accordingly, the NWs with $d > d_{crit}$ can serve as a platform for fundamentally investigating the correlation between the SBB and the molecule adsorption/metal NP decoration on the NW surfaces.

We first demonstrate that most ZnO NWs used here are incompletely depleted *via* the evidence that an NW with a relatively small diameter is incompletely depleted. On the basis of SEM analysis (Figure 2a), the distribution of NW diameters can be obtained with a mean value of 250 nm (Figure 2b). To meet the criterion of eq 2, we choose a relatively small NW [whose diameter is smaller than that of most NWs (~90%)] to characterize the NW FET performance in ambient atmosphere. The top inset in Figure 2c shows an SEM image of the FET device, where the diameter of the NW is 150 nm and the length between the electrodes is 2.86 μm. The drain current−gate voltage (I_d−V_g) curve shown in Figure 2c yields a threshold gate voltage (V_{th}) of −4.83 V, indicating that the ZnO NW FET is in normally on-type depletion mode. Note that the V_{th} is defined as the gate voltage obtained by extrapolating the linear

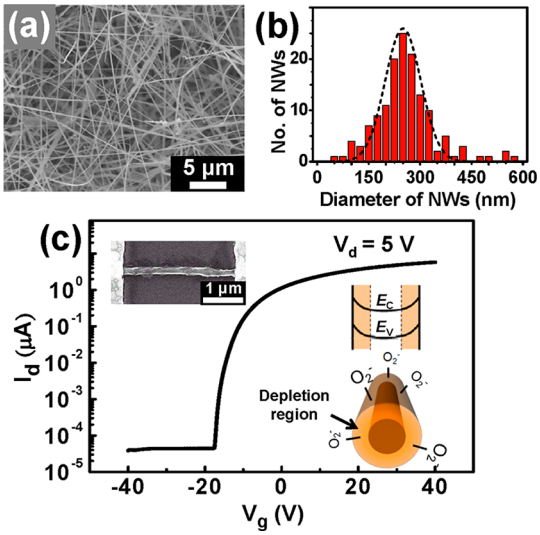

Figure 2. (a) SEM image of ZnO NWs, (b) distribution of the diameter of NWs extracted from (a), and (c) I_d-V_g curve of a single ZnO NW at V_d = 5 V. The top inset is an SEM image of the NW FET with 150 nm diameter. The right inset in (c) shows the schematic of the band diagram for the oxygen-adsorbed ZnO NW. E_C and E_V represent conduction band minimum and valence band maximum, respectively.

portion of the I_d-V_g characteristics from the point of maximum slope to zero drain current, in which the point of maximum slope is the point where transconductance ($g_m = dI_d/dV_g$) is maximal. This result proves that the device is incompletely depleted at zero gate bias. Since over 90% of the as-grown ZnO NWs are thicker than 150 nm, we can conclude that most of the ZnO NWs are incompletely depleted. In addition, by assuming that the NW is a cylinder on an infinite metal plate, the carrier concentration (n) of the NW can be obtained by[1,26]

$$n = \frac{C_g|V_g - V_{th}|}{e\pi r^2 L} \quad (3)$$

where the capacitance (C_g) per unit length is $((2\pi\varepsilon_{SiO_2}\varepsilon_0 L)/(\cosh^{-1}(r + h/r)))$, ε_{SiO_2} is the dielectric constant of the SiO_2 (3.9), ε_0 is the permittivity of free space, h is the oxide layer thickness, r is NW radius, and L is channel length. Using the experimental parameters, the carrier concentration is estimated to be $\sim 7.9 \times 10^{17}$ cm^{-3} at V_g = 0 V.

The Fermi level (E_F) position in our NWs is critical to determine the SBB by photoelectron spectroscopy, as shown in Figure 3. For nondegenerated semiconductor, the E_F in the core of NW can be determined by[12]

$$\xi = E_C - E_F = kT\ln(N_C/n) \quad (4)$$

where E_C is the conduction band minimum, k is Boltzmann constant, T is Kelvin temperature, and N_C is the conduction band density of states = 2.94×10^{18} cm^{-3}.[12] As the temperature is 300 K, the E_F lies 0.034 eV below the E_C (*i.e.*, $\xi = E_C - E_F$ = 0.034 eV).

The *in situ* UPS measurements were performed on our NWs in the following conditions: (A) the NWs

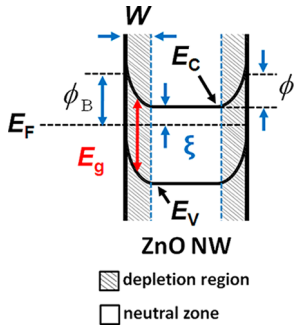

Figure 3. Band diagram of incompletely depleted ZnO NWs with conduction band minimum (E_C), valence band maximum (E_V), Fermi level energy (E_F), surface band bending (φ), surface barrier height (φ_B), and width of the SBB region (W). The relative energetic locations of E_C, E_V, and E_F are not on scale.

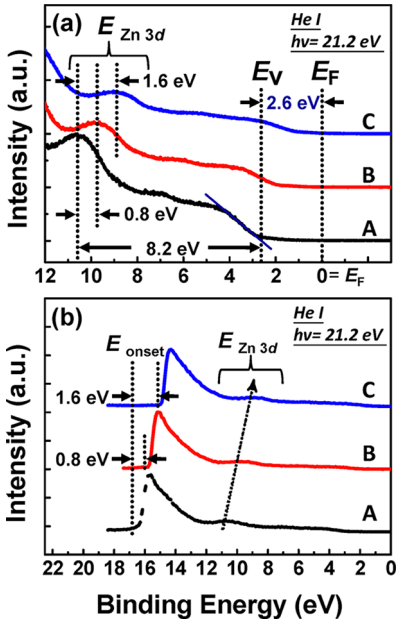

Figure 4. (a) UPS spectra, near the Fermi level energy and valence band maximum, of ZnO NWs with different surface conditions, *i.e.*, (A) NWs at 100 °C (namely, pristine ZnO NWs without oxygen adsorption), (B) NWs at room temperature (namely, oxygen molecule-adsorbed ZnO NWs), and (C) NWs with Au NP decoration at room temperature (namely, Au NP-decorated ZnO NWs). (b) Whole UPS spectra.

at 100 °C (*i.e.*, NWs without oxygen adsorbates), (B) the NWs at room temperature (*i.e.*, oxygen-adsorbed NWs), and (C) the Au NP-decorated NWs at room temperature (*i.e.*, further enhancing the oxygen adsorption for NWs), as shown in Figure 4. Since the UPS detection depth is ~1−3 nm, the shifts that we observe in the ZnO spectra can be attributed to the changes in the valence band minimum near the surface ($E_{V,S}$) of NWs due to the band bending at the surface. To inspect the SBB of ZnO NWs by the UPS technique, the energy difference between the $E_{V,S}$ to the E_F near the surface is measured. As shown schematically in Figure 3, the SBB of NWs can be determined by[31,32]

$$\phi = \phi_B - \xi = E_g - (E_F - E_{V,S}) - \xi \quad (5)$$

where ϕ_B represents the surface barrier height, E_g is the energy band gap of ZnO, and ξ is the energy difference between E_F and E_c near the core. As mentioned previously, the E_F of bulk ZnO is 0.034 eV below the E_C (*i.e.*, $\xi = E_C - E_F = 0.034$ eV). For pristine NWs at 100 °C (curve A), the heat treatment removed most of the adsorbed oxygen molecules from the NW surface. By heating the ZnO NW to eliminate the interference from oxygen, it is found that the $E_{V,S}$ is located at 2.6 eV below E_F by linearly extrapolating the leading edge of the valence band spectrum to the baseline. According to eq 5, the SBB of the ZnO NWs without adsorbed oxygen molecules is estimated to be 0.74 ± 0.15 eV [$\phi = \phi_B - \xi = E_g - (E_F - E_{V,S}) - \xi = 3.37 - 2.6 - 0.034 \cong 0.74$]. The error bar is from the UPS resolution of ~0.15 eV. This upward SBB originates from residual adsorbed oxygen molecules, high natural doping, and extremely high density of surface states due to the large surface-to-volume ratio of ZnO NWs.[22] Note that the difference of SBB caused by the temperature change would be approximately 0.1 eV.[21,33] Moreover, the peak located at around 10.6 eV originates from the Zn 3d core level; the energy difference between the Zn 3d peak and the $E_{V,S}$ is 8.2 eV, consistent with the value measured in the previous reports.[34,35] Furthermore, we do note that for the surface-modified NWs (curves B and C), direct and accurate determination of $E_{V,S}$ by the photoemission technique often becomes difficult. It is because the features caused by oxygen adsorption (*i.e.*, O 2p feature located at around 2−4 eV)[32,34] and Au decoration (*i.e.*, Au 5d band located at around 4 to 8 eV)[31,32] tend to dominate in the high kinetic energy region of the spectrum and obscure the signal from the $E_{V,S}$ of ZnO.

In Figure 4a, as compared with the curve A, the shifts of the Zn 3d peak for the curves B and C are −0.8 and −1.6 eV, respectively. To ascertain whether the shifts of the binding energies are valid and correctly measured, it must be confirmed that these shifts of the Zn 3d peak are equal to the shifts for each onset level (E_{onset}), which represents the deepest energy level where the electrons can be extracted in the valence band,[36] as shown in Figure 4b. Note that the peaks near the onset levels are caused by the secondary electrons instead of the electrons emitted from the valence band. These E_{onset} shifts observed in the spectra can be attributed to the changes in the NW work function (Φ) caused by SBB. The Φ can be calculated by[36]

$$\Phi = h\nu - E_{onset} \quad (6)$$

where $h\nu$ is 21.2 eV, representing the incident photon energy. Furthermore, the modified valence band minimum near the surface ($E'_{V,S}$) due to oxygen adsorption/Au NP decoration can be obtained by

$$E'_{V,S} = E_V + \Delta E \quad (7)$$

where ΔE is the energy shift for the Zn 3d peak or the E_{onset}. Therefore, the SBB of the oxygen-adsorbed ZnO

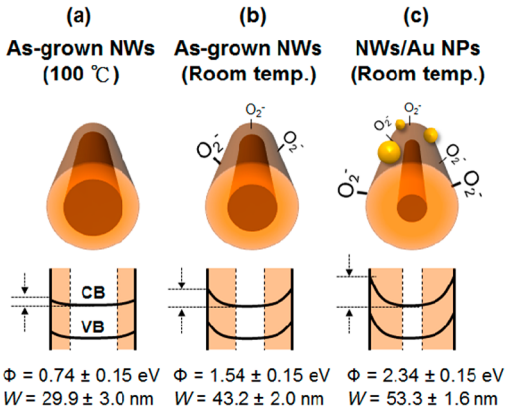

Figure 5. Schematic of surface band bending for (a) NWs without oxygen adsorption, (b) oxygen-adsorbed NWs, and (c) NWs with Au NP decoration for enhancing oxygen adsorption. E_C and E_V are conduction band minimum and valence band maximum, respectively.

NWs is estimated to be ~1.54 ± 0.15 eV. Physically speaking, as oxygen molecules adsorb on the NW surfaces and form negative ions by capturing electrons inside the NWs [$O_2(g) + e^- \rightarrow O_2^-(ad)$], a low conductivity depletion layer is formed near the surface, leading to more upward SBB.[3,9−11] The adsorbed oxygen molecules change upwardly the band bending at the nonpolar surfaces (*i.e.*, *m*-plane or *a*-plane) of the *c*-axis-oriented ZnO NWs by 0.8 eV.

To confirm the spectral shift resulting from the SBB, the ZnO NWs were deposited with Au NPs and the resulting spectral changes are shown in curve C in Figure 4. We observe a spectral shift to lower binding energy. Similarly, 2.34 ± 0.15 eV of the SBB for the Au NP-decorated ZnO NWs can be determined by eqs 5 and 7. A comparison of the SBB in different conditions is shown in Figure 5. It is noteworthy that the measured value is higher than the ideally predicted value based on the electron affinity rule ($\phi_B = \Phi_M - \chi_S = 1.2$ eV; Φ_M is the work function of Au; χ_S is the electron affinity of ZnO),[34,37,38] and the reported value (ϕ_B = 0.7−1.2 eV) measured from typical *IV* and *CV* measurements.[18−20] Several concepts are invoked to the unusually high band bending for Au NP-decorated ZnO surfaces: (1) according to Schottky−Mott theory, electrons flow from the ZnO NWs to the Au NPs until both the Fermi levels line up, leading to the open-circuit nano-Schottky junctions;[30,39] (2) due to the ~40% coverage rate of randomly distributed Au NPs, there are still oxygen molecules on the NW surfaces capturing electrons inside the NWs and altering the surface Fermi level of the NWs;[3,9−11] (3) spillover effect: Au NPs catalytically activate the formation of charged oxygen molecules, greatly increasing the quantity of oxygen adsorbates at the surface of ZnO NWs.[29,30,40] Due to the combination of the above effects, a greater amount of electrons drawn from the core of the Au NP-decorated NWs than the pristine NWs can be obtained, giving rise to the severe band bending.[12,22] Au NPs at

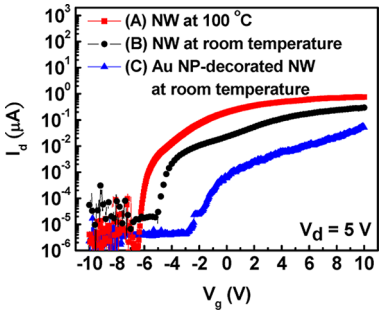

Figure 6. I_d–V_g curve of the ZnO NW with ~140 nm in diameter at V_d = 5 V under different conditions: (A) NW at 100 °C (*i.e.*, the NW without oxygen adsorbates), (B) NW at room temperature (*i.e.*, the oxygen-adsorbed NW), and (C) Au NP-decorated NW at room temperature (*i.e.*, further enhancing the oxygen adsorption for the NW).

ZnO surfaces creating Schottky junctions and enhancing the formation of the oxygen adsorbates amplify the separation of electron–hole pairs and further enhance the UV photogain of ZnO NW PDs.[29] Additionally, we do note that the enhanced photogain by Au decoration could cause from either (1) the increased oxygen absorption on the surface due to the presence of Au[29,30] or (2) the surface plasmon-enhanced light absorption by the decorated Au nanopartices.[41] El-Sayed *et al.* reported that with decreasing diameter of Au NP (from 99 to 9 nm) the plasmon absorption maximum is shifted to shorter wavelength (from 575 to 517 nm).[42] Accordingly, the surface plasmon-enhanced enhanced photosensitivity can be excluded in UV detection (lower than 370 nm) of ZnO NWs with Au NPs.[29] Moreover, the width of the SBB region (W) of our NWs (as shown in Figure 3) also can be calculated by[26]

$$W = \left(\frac{2\varepsilon_{ZnO}\varepsilon_0\phi}{en}\right)^{1/2} \quad (8)$$

where ε_{ZnO} is the dielectric constant of ZnO (8.66). The width of the SBB regions of our NWs under the three different surface conditions are shown in Figure 5. We also have measured the drain current–gate voltage (I_d–V_g) characteristics of the NW FET with ~140 nm in diameter under the different conditions: (A) the NW at 100 °C (*i.e.*, the NW without oxygen adsorbates), (B) the NW at room temperature (*i.e.*, the oxygen-adsorbed NW), and (C) the Au NP-decorated NW at room temperature (*i.e.*, further enhancing the oxygen adsorption for the NW), as shown in Figure 6 to have direct comparison of the electrical characteristics of the nanowire FET with the band bending model proposed based on the UPS data. The I_d–V_g curves exhibit three threshold gate voltages (V_{th}): −3.48, −1.025, and −0.12 V for (A) the NW at 100 °C, (B) the NW at room temperature, and (C) the Au NP-decorated NW at room temperature, indicating the ZnO NW FET under the different conditions always is in normally on-type depletion mode. This result shows that the controlled surface effects can lead to electrical tunability, for example, V_g shift, and proves that the NW under the different conditions always is incompletely depleted at zero gate bias. Due to the average diameter of ~250 nm for our NWs, most of our NWs would be incompletely depleted under these surface conditions. Additionally, according to the absolute value of the three threshold voltages, it is estimated that the width of the SBB region for (A) the NW at 100 °C < that of (B) the NW at room temperature < that of (C) the Au NP-decorated NW at room temperature,[27,43] which is consistent with the band bending model proposed based on the UPS data.

CONCLUSIONS

We utilized the FET analyses and the *in situ* UPS to quantitatively investigate the correlation between the SBB of the ZnO NWs and the surface conditions. It is found that a 100 °C heat treatment is able to remove most adsorbed oxygen molecules, reducing the SBB to 0.74 ± 0.15 eV with the width of 29.9 ± 3.0 nm. The SBB of the oxygen-adsorbed ZnO NWs is 1.54 ± 0.15 eV with the width of 43.2 ± 2.0 nm. Moreover, the decoration of Au NPs on the ZnO NW surfaces can create nano-Schottky junctions and enhances the formation of the charge O_2 adsorbates, causing the unusually high SBB (2.34 ± 0.15 eV with the wide width of 53.3 ± 1.6 nm). Our study showing in-depth understanding of the surface effect can be generic to all metal oxide nanostructures and can provide the strategies for optimizing the performance of NW-based devices in sensor and optoelectronic applications *via* surface engineering.

EXPERIMENTAL SECTION

The fabrication procedure of the FET devices is as follows. ZnO NWs were prepared by heating mixed ZnO and C powders (6.6 g, 3.3 g) in the furnace at 930 °C for 1 h using the vapor–liquid–solid method. NWs were then transferred to Si substrates with a 600 nm thick SiO_2 layer. Contact electrodes were defined by electron beam lithography and then deposited by e-beam evaporation (Ti/Au: 10 nm/100 nm). The devices were annealed at 400 °C for 30 s in order to obtain ohmic contacts. Morphological observation was conducted with an ELIONIX-7500 electron beam lithography system operating at 50 kV with a nominal point-to-point resolution of 2 nm. Microstructures were examined using a JEOL 4000EX TEM operating at 400 kV with a nominal point-to-point resolution of 0.18 nm.

To achieve *in situ* measurements without exposure to external environment, photoemission experiments were carried out in two interconnected ultrahigh vacuum chambers; one is for the deposition, and the other is for the spectroscopy analysis. The Fermi level of the system was measured on a clean Au substrate. The ZnO NWs with ~5 Å thick Au decoration were prepared by e-beam evaporation in the deposition chamber and were then transferred to the analysis chamber. The nominal thickness of the Au NP layer was determined using a quartz crystal microbalance. A thermal controller was used to vary the

temperature in the analysis chamber. The band diagrams of ZnO NWs were analyzed by UPS. The valence band spectra were measured *via* He I (21.2 eV) as excitation sources at a base pressure at 10^{-10} Torr. The energy spectra of photoelectrons were collected with a cylindrical mirror analyzer with a resolution of ~0.15 eV.[44,45]

Conflict of Interest: The authors declare no competing financial interest.

Acknowledgment. This work was supported by National Science Council of Taiwan (99-2622-E-002-019-CC3, 99-2112-M-002-024-MY3, 101-2622-E-002-012-CC3, and 99-2120-M-007-011) and National Taiwan University (10R70823).

REFERENCES AND NOTES

1. Chen, C. Y.; Chen, M. W.; Ke, J. J.; Lin, C. A.; Retamal, J. R. D.; He, J. H. Surface Effect on Optical and Electrical Properties of ZnO Nanostructure. *Pure Appl. Chem.* **2008**, *82*, 2055–2073.
2. Chen, C. Y.; Chen, M. W.; Hsu, C. Y.; Lien, D. H.; Chen, M. J.; He, J. H. Enhanced Recovery Speed of Nanostructured ZnO Photodetectors Using Nanobelt Networks. *IEEE J. Sel. Top. Quantum Electron.* **2012**, *18*, 1807–1811.
3. Soci, C.; Zhang, A.; Xiang, B.; Dayeh, S. A.; Aplin, D. P. R.; Park, J.; Bao, X. Y.; Lo, Y. H.; Wang, D. ZnO Nanowire UV Photodetectors with High Internal Gain. *Nano Lett.* **2007**, *7*, 1003–1009.
4. Zhou, J.; Gu, Y. D.; Hu, Y. F.; Mai, W. J.; Yeh, P. H.; Bao, G.; Sood, A. K.; Polla, D. L.; Wang, Z. L. Gigantic Enhancement in Response and Reset Time of ZnO UV Nanosensor by Utilizing Schottky Contact and Surface Functionalization. *Appl. Phys. Lett.* **2009**, *94*, 191103.
5. Li, L.; Lee, P. S.; Yan, C. Y.; Zhai, T. Y.; Fang, X. S.; Liao, M. Y.; Koide, Y.; Bando, Y.; Golberg, D. Ultrahigh-Performance Solar-Blind Photodetectors Based on Individual Single-Crystalline $In_2Ge_2O_7$ Nanobelts. *Adv. Mater.* **2010**, *22*, 5145–5149.
6. Park, W.; Jo, G.; Hong, W.-K.; Yoon, J.; Choe, M.; Lee, S.; Ji, Y.; Kim, G.; Kahng, Y. H.; Lee, K.; *et al.* Enhancement in the Photodetection of ZnO Nanowires by Introducing Surface-Roughness-Induced Traps. *Nanotechnology* **2011**, *22*, 205204.
7. Ko, H.; Takei, K.; Kapadia, R.; Chuang, S.; Fang, H.; Leu, P. W.; Ganapathi, K.; Plis, E.; Kim, H. S.; Chen, S. Y.; *et al.* Ultrathin Compound Semiconductor on Insulator Layers for High Performance Nanoscale Transistors. *Nature* **2010**, *468*, 286–289.
8. Fan, Z.; Wang, D.; Chang, P. C.; Tseng, W. Y.; Lu, J. G. ZnO Nanowire Field-Effect Transistor and Oxygen Sensing Property. *Appl. Phys. Lett.* **2004**, *85*, 5923–5925.
9. Chen, C. Y.; Lin, C. A.; Chen, M. J.; Lin, G. R.; He, J. H. ZnO/Al_2O_3 Core–Shell Nanorod Arrays: Growth, Structural Characterization, and Luminescent Properties. *Nanotechnology* **2009**, *20*, 185605.
10. He, J. H.; Chang, P. H.; Chen, C. Y.; Tsai, K. D. Electrical and Optoelectronic Characterization of ZnO Nanowire Contacted by Focused-Ion-Beam-Deposited Pt. *Nanotechnology* **2009**, *20*, 135701.
11. He, J. H.; Ho, C. H.; Chen, C. Y. Polymer Functionalized ZnO Nanobelt as Gas Sensor with a Significant Response Enhancement. *Nanotechnology* **2009**, *20*, 065503.
12. Allen, M. W.; Durbin, S. M. Influence of Oxygen Vacancies on Schottky Contacts to ZnO. *Appl. Phys. Lett.* **2008**, *92*, 122110.
13. Zhai, T.; Fang, X.; Liao, M.; Xu, X.; Zeng, H.; Yoshio, B.; Golberg, D. A Comprehensive Review of One-Dimensional Metal-Oxide Nanostructure Photodetectors. *Sensors* **2009**, *9*, 6504–6529.
14. Soci, C.; Zhang, A.; Bao, X. Y.; Kim, H.; Lo, Y.; Wang, D. Nanowire Photodetectors. *J. Nanosci. Nanotechnol.* **2010**, *10*, 1430–1449.
15. Hsu, C. Y.; Lien, D. H.; Lu, S. Y.; Chen, C. Y.; Kang, C. F.; Chueh, Y. L.; Hsu, W. K.; He, J. H. A Supersensitive, Ultrafast, and Broadband Light-Harvesting Scheme Employing Carbon Nanotube/TiO_2 Core–Shell Nanowire Geometry. *ACS Nano* **2012**, *6*, 6687–6692.
16. Huang, J.; Wan, Q. Gas Sensors Based on Semiconducting Metal Oxide One-Dimensional Nanostructures. *Sensors* **2009**, *9*, 9903–9924.
17. Chen, P. C.; Shen, G.; Zhou, C. Chemical Sensors and Electronic Noses Based on 1-D Metal Oxide Nanostructures. *IEEE Trans. Nanotechnol.* **2008**, *7*, 668–682.
18. Coppa, B. J.; Davis, R. F.; Nemanich, R. J. Gold Schottky Contacts on Oxygen Plasma-Treated, n-Type ZnO($000\bar{1}$). *Appl. Phys. Lett.* **2003**, *82*, 400.
19. Allen, M. W.; Alkaisi, M. M.; Durbin, S. M. Metal Schottky Diodes on Zn-Polar and O-Polar Bulk ZnO. *Appl. Phys. Lett.* **2006**, *89*, 103520.
20. Dong, Y.; Fang, Z. Q.; Look, D. C.; Cantwell, G.; Zhang, J.; Song, J. J.; Brillson, L. J. Zn- and O-Face Polarity Effects at ZnO Surfaces and Metal Interfaces. *Appl. Phys. Lett.* **2008**, *93*, 072111.
21. Das, S. N.; Choi, J. H.; Kar, J. P.; Moon, K. J.; Lee, T. I.; Myoung, J. M. Junction Properties of Au/ZnO Single Nanowire Schottky Diode. *Appl. Phys. Lett.* **2010**, *96*, 092111.
22. Tung, R. T. Recent Advances in Schottky Barrier Concepts. *Mater. Sci. Eng., R* **2001**, *35*, 1.
23. Briggs, D.; Seah, M. P. *Practical Surface Analysis by Auger and X-ray Photoelectron Spectroscopy*: John Wiley & Sons: New York, 1983.
24. Wang, Z. L. ZnO Nanowire and Nanobelt Platform for Nanotechnology. *Mater. Sci. Eng., R* **2009**, *64*, 33–71.
25. Coppa, B. J.; Fulton, C. C.; Hartlieb, P. J.; Davis, R. F.; Rodriguez, B. J.; Shields, B. J.; Nemanich, R. J. *In Situ* Cleaning and Characterization of Oxygen- and Zinc-Terminated, n-Type, ZnO{0001} Surfaces. *J. Appl. Phys.* **2004**, *95*, 5856.
26. Calarco, R.; Marso, M.; Richter, T.; Aykanat, A. I.; Meijers, R.; v.d. Hart, A.; Stoica, T.; Lüth, H. Size-Dependent Photoconductivity in MBE-Grown GaN-Nanowires. *Nano Lett.* **2005**, *5*, 981.
27. Hong, W. K.; Jo, G.; Kwon, S. S.; Song, S.; Lee, T. Electrical Properties of Surface-Tailored ZnO Nanowire Field-Effect Transistors. *IEEE Trans. Electron Devices* **2008**, *55*, 3020–3029.
28. Lin, C. H.; Chen, T. T.; Chen, Y. F. Photocurrent Enhancement of SnO_2 Nanowires through Au-Nanoparticles Decoration. *Opt. Express* **2008**, *16*, 16916–16922.
29. Chen, M. W.; Chen, C. Y.; Lien, D. H.; Ding, Y.; He, J. H. Photoconductive Enhancement of Single ZnO Nanowire through Localized Schottky Effects. *Opt. Express* **2010**, *18*, 14836–14841.
30. Kolmakov, A.; Klenov, D. O.; Lilach, Y.; Stemmer, S.; Moskovits, M. Enhanced Gas Sensing by Individual SnO_2 Nanowires and Nanobelts Functionalized with Pd Catalyst Particles. *Nano Lett.* **2005**, *5*, 667–673.
31. Tracy, K. M.; Hartlieb, P. J.; Einfeldt, S.; Davis, R. F.; Hurt, E. H.; Nemanich, R. J. Electrical and Chemical Characterization of the Schottky Barrier Formed between Clean n-GaN (0001) Surfaces and Pt, Au, and Ag. *J. Appl. Phys.* **2003**, *94*, 3939.
32. Coppa, B. J.; Fulton, C. C.; Kiesel, S. M.; Davis, R. F.; Pandarinath, C.; Burnette, J. E.; Nemanich, R. J. Structural, Microstructural, and Electrical Properties of Gold Films and Schottky Contacts on Remote Plasma-Cleaned, n-Type ZnO{0001} Surfaces. *J. Appl. Phys.* **2005**, *97*, 103517.
33. Ip, K.; Heo, Y. W.; Baik, K. H.; Norton, D. P.; Pearton, S. J.; Kim, S.; LaRoche, J. R.; Ren, F. Temperature-Dependent Characteristics of Pt Schottky Contacts on n-Type ZnO. *Appl. Phys. Lett.* **2004**, *84*, 2835.
34. Jacobi, K.; Zwicker, G.; Gutmann, A. Work Function, Electron Affinity and Band Bending of Zinc Oxide Surfaces. *Surf. Sci.* **1984**, *141*, 109.
35. Hong, S. K.; Hanada, T.; Makino, H.; Chen, Y.; Ko, H. J.; Tanaka, A.; Sasaki, H.; Sato, S. Band Alignment at a ZnO/GaN (0001) Heterointerface. *Appl. Phys. Lett.* **2001**, *78*, 3349.
36. Klein, A.; Säuberlich, F.; Späth, B.; Schulmeyer, T.; Kraft, D. Non-stoichiometry and Electronic Properties of Interfaces. *J. Mater. Sci.* **2007**, *42*, 1890–1900.

37. Liang, S.; Sheng, H.; Liu, Y.; Huo, Z.; Lu, Y.; Shen, H. ZnO Schottky Ultraviolet Dhotodetectors. *J. Cryst. Growth* **2001**, *225*, 110.
38. Michaelson, H. B. The Work Function of the Elements and Its Periodicity. *J. Appl. Phys.* **1977**, *48*, 4729.
39. Zhdanov, V. P. nm-Sized Metal Particles on a Semiconductor Surface, Schottky Model, *etc. Surf. Sci.* **2002**, *512*, L331–L334.
40. Khoobiar, S. Particle to Particle Migration of Hydrogen Atoms on Platinum−Alumina Catalysts from Particle to Neighboring Particles. *J. Phys. Chem.* **1964**, *68*, 411–412.
41. Schaadt, D. M.; Feng, B.; Yu, E. T. Enhanced Semiconductor Optical Absorption *via* Surface Plasmon Excitation in Metal Nanoparticles. *Appl. Phys. Lett.* **2005**, *86*, 063106.
42. Link, S; El-Sayed, M. A. Size and Temperature Dependence of the Plasmon Absorption of Colloidal Gold Nanoparticles. *J. Phys. Chem. B* **1999**, *103*, 4212–4217.
43. Maeng, J.; Jo, G.; Kwon, S.-S.; Song, S.; Seo, J.; Kang, S. J.; Kim, D. Y.; Lee, T. Effect of Gate Bias Sweep Rate on The Electronic Properties of ZnO Nanowire Field Effect Transistors under Different Environment. *Appl. Phys. Lett.* **2008**, *92*, 233120.
44. Wu, C. I; Lin, C. T.; Chen, Y. H.; Chen, M. H.; Lu, Y. J.; Wu, C. C. Electronic Structures and Electron-Injection Mechanisms of Cesium-Carbonate-Incorporated Cathode Structures for Organic Light-Emitting Devices. *Appl. Phys. Lett.* **2006**, *88*, 152104.
45. Chen, M. H.; Chen, Y. H.; Lin, C. T.; Lee, G. R.; Wu, C. I.; Leem, D. S.; Kim, J. J.; Pi, T. W. Electronic and Chemical Properties of Cathode Structures Using 4,7-Diphenyl-1,10-phenanthroline Doped with Rubidium Carbonate as Electron Injection Layers. *J. Appl. Phys.* **2009**, *105*, 113714.